Lawrence Berkeley National Laboratory

Title

Functional Materials Under Stress: In Situ TEM Observations of Structural Evolution

Permalink

Journal

ISSN

Authors

Deng, Yu
Zhang, Ruopeng
Pekin, Thomas C
et al.

Publication Date

DOI

Peer reviewed

Functional materials under stress: *in-situ* TEM observations of structural evolution

Yu Deng[a,†,*], Ruopeng Zhang[b,c,†], Thomas C. Pekin[b,c], Christoph Gammer[d], Jim Ciston[b], Colin Ophus[b], Peter Ercius[b], Karen Bustillo[b], Chengyu Song[b], Shiteng Zhao[b,c], Hua Guo[e], Yunlei Zhao[a], Hongliang Dong[f], Zhiqiang Chen[f,†] & Andrew M. Minor[b,c]

[a]*Solid State Microstructure National Key Lab and Collaborative Innovation Center of Advanced Microstructures, Nanjing University, Nanjing 210093, China*

[b]*National Center for Electron Microscopy, Molecular Foundry, Lawrence Berkeley National Laboratory, Berkeley, California 94720, USA*

[c]*Department of Materials Science & Engineering, University of California, Berkeley, California 94720, USA*

[d]*Erich Schmid Institute of Materials Science, Austrian Academy of Sciences, Jahnstrasse 12, 8700, Leoben, Austria*

[e] *Department of Materials Science & NanoEngineering, Rice University, Houston, Texas 77251, USA*

[f]*Center for High Pressure Science and Technology Advanced Research, Shanghai 201203, China*

[†] *These authors contributed equally to this work.*

[*] *Correspondence to dengyu@nju.edu.cn*

Abstract

The operating conditions of functional materials usually involve varying stress fields resulting in either intentional or undesirable structural changes. Complex multiscale microstructures, including defects, domains and new phases in functional materials can be induced in situ by mechanical loading, providing fundamental insight into their deformation process. The resulting microstructure, if induced in a controllable fashion, can be used to tune the functional properties or to enhance their performance. *In-situ* nanomechanical testing conducted in (Scanning) Transmission Electron Microscopes (STEM/TEM) provides a

critical tool for understanding the microstructural evolution in functional materials. In this report, select results from a variety of functional materials systems will be presented in the context of newly developed multi-modal experimental capabilities to demonstrate the impact of these techniques.

1. Introduction

The properties of functional materials are strongly determined by the underlying microstructure, which is usually sensitive to the operating conditions during specific applications. Observing and characterizing the dynamic process of the microstructural evolution is therefore critical for the understanding of their structure-property relationship[1–8]. It is also possible to tune the performance of materials via microstructural engineering by applying external electrical, magnetic or thermal fields and mechanical loading[9–18]. Thanks to the development of *in-situ* (S)TEM testing, new capabilities for conducting nano-scale *in-situ* observation of materials' microstructure evolution have become increasingly available[8,19,20]. Among these external stimuli, nanomechanical deformation features high stress levels that cannot be easily achieved in macroscopic testing. High stresses result in complex microstructures [21–26] that span multiple length scales[9,21,24,27–33]. Understanding these stress-induced phenomena can provide valuable insight into the performance of the materials and illuminate the potential for novel functional micro/nano-device applications.

Quantitative application and measurement of stresses and strains during *in-situ* TEM nanomechanical testing is now routine [34–39]. Coupled with the on-going adoption of aberration-corrected (S)TEM instruments, it is possible to achieve atomic resolution during *in-situ* experiments[1,4,19,20]. Therefore, atomic-scale features and defects can be directly observed during *in-situ* STEM experiments[40,41]. As an emerging data-intensive STEM technique, nano-

beam electron diffraction (NBED, also called 4D-STEM) combines the benefits of a finely-focused electron probe and the information-rich diffraction patterns[42–45]. Direct electron detector (DED) cameras can operate at thousands of frames per second, enabling time-resolved *in-situ* 4D-STEM experiments[46–51], from which multi-modal characterization can be extracted from a single experimental dataset. Examples include orientation mapping[44,45], strain evolution[52,53], and local structural ordering[50]. As *in-situ* nanomechanical testing is usually conducted irreversibly, the multi-channel nature of 4D-STEM is essential to capture more of the information during dynamic processes. Aside from the advances of TEM instruments and analytical methods, more sophisticated micro-electro-mechanical devices (MEMS) have been incorporated into *in-situ* nano mechanical testing[54–59], some of which have capabilities for applying and measuring fields along with mechanical load.

In this report, we showcase some recent progress of *in-situ* (S)TEM nanomechanical testing with emphasis on functional materials.

2. *In-situ* functionality measurement during mechanical loading

Ferroics are a widely used class of functional materials, demonstrating both ferroelectric and ferroelastic properties. Stress-induced domain evolution or phase transformations provide an effective way to alter the electrical properties of a ferroic. As shown in Figure 1, a stress-induced insulating-to-conductive domain structure evolution in an individual $BaTiO_3$ nanopillar has been revealed via *in-situ* TEM observation. The pillar originally displayed a herringbone domain structure, which transformed into a common (head-to-tail) 180-degree domain structure under axial tension or a head-to-head charged 180-degree domain structure under axial compression[60]. The strongly charged head-to-head 180-degree domain wall is in fact a free-electron gas structure, exhibiting metallic-type conductivity that is 10^9 times higher than the parent $BaTiO_3$ crystal[61,62]. However, the 2-dimensional domain wall structure is inherently

unstable at equilibrium owing to its higher energy[61]. Here the structure is not formed until the compression load reaches 280 MPa (Figure 1(a)). A steady conductivity between the pillar substrate and the boron-doped conductive nanoindentation tip was achieved with the applied mechanical stress (Figure 1(b)). Notably, the stress-induced charged head-to-head domain wall (i.e. the free-electron gas structure) was not present in the entire nanopillar at first yet showing a "deflecting growth" which avoided approaching the top electrode of the pillar, until a 4V voltage was applied (Figure 1(c)). Such behavior is theoretically predicted (an energy barrier must be overcome before the head-to-head domain wall connecting the electrodes subsequently enables current)[61], but rarely reported via direct experimental observation. It is worth mentioning that unlike heterogeneous interfaces, domain walls in ferroelectrics can be created, displaced, annihilated and recreated via reversible mechanical loading.

An ongoing pursuit of *in-situ* nanomechanical TEM experimental systems is the integration of multi-modal measurements during the loading process. Examples include the measurements of electrical[63,64] and/or thermal[56] properties while applying a mechanical load to the sample. Zhang et al. observed a large electric field-induced strain in $BiFeO_3$ using a commercially available MEMS-based system and demonstrated the potential of the material in piezoelectric applications[63]. Gao et al. revealed a ferroelastic domain-wall-mediated ferroelectric switching in $Pb(Zr_{0.2}Ti_{0.8})O_3$ thin films using a customized systems[64]. Controllable thermal fields can be applied using a resistive heater, by Joule heating of the material, or by electron-beam heating[56].

3. Application of 4D-STEM during *in-situ* nanomechanical testing

4D-STEM is a diffraction based technique that has the potential to combine high spatial resolution (~1nm) with a large field of view (~1μm)[42,43,45]. To acquire a 4D-STEM dataset, one needs to work in the STEM mode, where the electron probe scans through the area of

interest and the diffraction pattern is recorded at each scanning position. The 4D-STEM dataset contains a 2D array of spatial positions, each containing a full 2D reciprocal-space diffraction pattern, resulting in a 4D dataset[45]. Therefore, one 4D-STEM acquisition could be used for virtual-aperture diffraction contrast bright-field/dark-field (BF/DF) imaging[42], orientation mapping[44,65], large-field-of-view strain mapping[43] and even local chemical ordering mapping[50,66]. The operating principle of 4D-STEM is demonstrated in Figure 2(a) along with an experimental example of a $SrTiO_3/PbTiO_3$ multilayer heterojunction by a multiple-channel acquisition on composition, strain and polarization mapping[67]. The application of 4D-STEM during *in-situ* experiments has been significantly expanded recently thanks to the deployment of fast DED camera with frame rates up to ~thousands of frames per second level[46,47,51,68]. The fast readout speed is important, not just for increased scan speed, but also for the opportunity to probe dynamic events during *in-situ* STEM/TEM studies[48–50,69]. Figure 2(b) further demonstrates the advantages of NBED in *in-situ* experiments[70], where multi-modal contrast can be achieved with a single dataset, simplifying the experimental workflow of *in-situ* nanomechanical testing and enabling more dynamic correlation analysis.

Considering the information-rich characteristic of the 4D-STEM, it is likely that the technique will be increasing utilized to characterize functional materials, especially for *in-situ* dynamic observations.

4. Atomic-resolution imaging during *in-situ* nanomechanical testing

One recent trend of *in-situ* (S)TEM nanomechanical testing is to approach the atomistic mechanism of microstructural evolution[71–74], in which the *in-situ* mechanical tests are conducted via atomic-resolution (S)TEM imaging. At the atomic level, the dynamic microstructural evolution becomes evident at the level of individual defects or features on the order of a single-unit-cell size, revealing atomistic insight on the materials' properties.

Figure 3 shows an *in-situ* atomic resolution observation of a crystalline $BaTiO_3$ nanopillar under a shear load. We found that defects nucleated in the $BaTiO_3$ nanopillar at a 90-degree domain wall, as the local shearing stress goes up to ~2GPa. The deformation mechanism of the $BaTiO_3$ pillar was observed as follows[75]: (1) For stress release, the 90-degree domain wall was easily induced in $BaTiO_3$ (as the stress approached 10 MPa); (2) Mobile point defects (mainly oxygen vacancies in $BaTiO_3$[15]) then accumulated at the domain walls, providing sites for dislocation nucleation[31,32]; (3) As the stress further increased to ~2 GPa, more dislocations nucleated at the 90-degree domain wall, subsequently triggering the cracking along the domain wall[60].

5. MEMS-based *in-situ* (S)TEM nanomechanical testing

The design of *in-situ* (S)TEM mechanical tests are often constrained by the limited space in a TEM column (the vertical gap between objective pole pieces in which the sample sits in a TEM is typically no more than 5 - 10 millimeters high). MEMS-based sample stages or single use devices have been widely integrated into *in-situ* TEM tests due to their small size and design flexibility[19,20,76–80]. For example, Figure 4(a) shows a simple passive push-to-pull (PtP) device, with a Si frame designed to turn compression of the device into tension at the sample[56,81]. The local phase transition of a VO_2 nanowire under heating has been probed by electron diffraction and dark-field imaging (Figure 4(b)). Owing to the volume change caused by the phase transition, there are corresponding strains and stresses generated inside the sample. By using the PtP device, the respond speed and the stress output have been measured *in-situ* (Figure 4(c)), revealing the potential of nanowires as actuators.

For *in-situ* testing of functional materials, maturity of MEMS fabrication would enable more sophisticated multi-channel chip designs (also known as "lab on a chip")[1,20]. Examples include the commercially-available e-PtP devices (simultaneous application of electrical and

mechanical fields)[20,78,79], and the *in-situ* TEM tensile device based on thermally actuated bimetallic strips[34]. In the future, highly integrated chip devices will be a solution for the next-generation mechanical *in-situ* TEM/STEM techniques, which results in more functionalities, lower experimental cost and easier experimental control[57].

6. *In-operando* functional device testing

Integrated devices enable the miniaturization of functional material devices[82,83]. Testing the performance or observing the failure mechanism of such ultra-small devices *in operando* has proven to be challenging as conventional characterization fails to provide a sufficient spatial resolution. Thus, *in-situ* TEM testing is an optimal way to assist in the development phase of ultra-small devices[20,81,82].

Figure 5(a) shows the cycling test of a VO_2 nanowire-based thermometer, which was used to monitor the heating effect of the electron beam[81] . Guo et al. utilized the metal-insulator transition (MIT) temperature of vanadium dioxide at 68 °C to construct a nanowire-based thermometer, which could be used as a thermal flow meter. 100 heating/cooling cycles (by blanking/unblanking the electron beam) were conducted to test the reliability of the device with respect to the residual strain output after the cycling.

As another example of a miniature device, Figure 5(b) shows a multiple-domain-structured $BaTiO_3$ nanopillar, which can function as a piezoelectric actuator. Interestingly, it shows an enhanced strain output after mechanical aging. Here, many nanodomains have been introduced into the nanopillar via compression and then stabilized by a time-dependent point defect pinning effect[11,33,75]. This is a 'domain engineering' effect[13,14] used to improve the piezoelectric response.

With the recent development of environmental *in-situ* TEM techniques, more *in operando* conditions can be applied (e.g. temperature, gases or radiation) simultaneously with external mechanical loading[20,84].

7. Summary and Prospects

We have highlighted a selection of recent advances in the field of *in-situ* (S)TEM nanomechanical testing for functional materials. Any functional material that involves mechanical properties in their potential service could benefit from *in-situ* (S)TEM nanomechanical testing-based observation. With the help of atomistic simulations[85,86], *in-situ* (S)TEM nanomechanical testing has the potential to accelerate the research and development of functional materials and functional materials-based applications.

Despite the significant progress, many opportunities remain unexplored in terms of instrument development, experimental techniques and analytical methods. In the near future, we believe that *in-situ* (S)TEM nanomechanical testing methods will continue to further evolve in the following aspects: (1) Incorporation with more *in-situ* capabilities such as magnetic field control and measurement, laser pump-probe, and environmental atmosphere. (2) Improved temporal resolution with the development of faster electron detectors and novel dynamic TEM techniques. (3) Fast and powerful data analysis tools for working with the high-bandwidth raw data associated with high spatial/temporal resolution or information-rich experimental methods such as 4D-STEM.

Received: ((will be filled in by the editorial staff))

Revised: ((will be filled in by the editorial staff))

Published online: ((will be filled in by the editorial staff))

References

[1] E. A. Stach, *Mater. Today* **2008**, *11*, 50.

[2] H. Liao, L. Cui, S. Whitelam, H. Zheng, *Science (80-.).* **2012**, *336*, 1011.

[3] R. M. Van Der Veen, O. H. Kwon, A. Tissot, A. Hauser, A. H. Zewail, *Nat. Chem.* **2013**, *5*, 395.

[4] M. L. Taheri, E. A. Stach, I. Arslan, P. A. Crozier, B. C. Kabius, T. LaGrange, A. M. Minor, S. Takeda, M. Tanase, J. B. Wagner, R. Sharma, *Ultramicroscopy* **2016**, *170*, 86.

[5] R. Sharma, *Micron* **2012**, *43*, 1147.

[6] Z. L. Wang, *Adv. Mater.* **2003**, *15*, 1497.

[7] Z. Liu, M. A. Monclús, L. W. Yang, M. Castillo-Rodríguez, J. M. Molina-Aldareguía, J. LLorca, *Extrem. Mech. Lett.* **2018**, *25*, 60.

[8] Z. Fan, L. Zhang, D. Baumann, L. Mei, Y. Yao, X. Duan, Y. Shi, J. Huang, Y. Huang, X. Duan, *Adv. Mater.* **2019**, DOI 10.1002/adma.201900608.

[9] T. T. A. Lummen, Y. Gu, J. Wang, S. Lei, F. Xue, A. Kumar, A. T. Barnes, E. Barnes, S. Denev, A. Belianinov, M. Holt, A. N. Morozovska, S. V. Kalinin, L. Q. Chen, V. Gopalan, *Nat. Commun.* **2014**, *5*, DOI 10.1038/ncomms4172.

[10] L. Kong, G. Liu, W. Yang, W. Cao, *Appl. Phys. Lett.* **2015**, *107*, 042901.

[11] X. Ren, *Nat. Mater.* **2004**, *3*, 91.

[12] S. Tsukada, T. H. Kim, S. Kojima, *APL Mater.* **2013**, *1*, DOI 10.1063/1.4821624.

[13] S. Wada, H. Kakemoto, T. Tsurumi, *Mater. Trans.* **2004**, *45*, 178.

[14] S. Wada, T. Muraishi, K. Yokoh, K. Yako, H. Kamemoto, T. Tsurumi, in *Ferroelectrics*, **2007**, pp. 37–49.

[15] J. C. Agar, A. R. Damodaran, M. B. Okatan, J. Kacher, C. Gammer, R. K. Vasudevan, S. Pandya, L. R. Dedon, R. V. K. Mangalam, G. A. Velarde, S. Jesse, N. Balke, A. M. Minor, S. V. Kalinin, L. W. Martin, *Nat. Mater.* **2016**, *15*, 549.

[16] Q. Yang, J. X. Cao, Y. C. Zhou, Y. Zhang, Y. Ma, X. J. Lou, *Appl. Phys. Lett.* **2013**, *103*, DOI 10.1063/1.4824215.

[17] Y. W. Li, X. B. Ren, F. X. Li, H. S. Luo, D. N. Fang, *Appl. Phys. Lett.* **2013**, *102*, DOI 10.1063/1.4795330.

[18] J. Paul, T. Nishimatsu, Y. Kawazoe, U. V. Waghmare, *Phys. Rev. B - Condens. Matter Mater. Phys.* **2009**, *80*, DOI 10.1103/PhysRevB.80.024107.

[19] Q. Yu, M. Legros, A. M. Minor, *MRS Bull.* **2015**, *40*, 62.

[20] A. M. Minor, G. Dehm, *MRS Bull.* **2019**, *44*, 438.

[21] G. Catalan, J. Seidel, R. Ramesh, J. F. Scott, *Rev. Mod. Phys.* **2012**, *84*, 119.

[22] J. F. Scott, *Science (80-.).* **2007**, *315*, 954.

[23] H. Lu, C. W. Bark, D. Esque De Los Ojos, J. Alcala, C. B. Eom, G. Catalan, A. Gruverman, *Science (80-.).* **2012**, *335*, 59.

[24] R. J. Zeches, M. D. Rossell, J. X. Zhang, A. J. Hatt, Q. He, C. H. Yang, A. Kumar, C. H. Wang, A. Melville, C. Adamo, G. Sheng, Y. H. Chu, J. F. Ihlefeld, R. Erni, C. Ederer, V. Gopalan, L. Q. Chen, D. G. Schldin, N. A. Spaldin, L. W. Martin, R. Ramesh, *Science (80-.).* **2009**, *326*, 977.

[25] L. W. Chang, V. Nagarajan, J. F. Scott, J. M. Gregg, *Nano Lett.* **2013**, *13*, 2553.

[26] Y. M. Jin, Y. U. Wang, A. G. Khachaturyan, J. F. Li, D. Viehland, *J. Appl. Phys.* **2003**, *94*, 3629.

[27] Z. W. Shan, G. Adesso, A. Cabot, M. P. Sherburne, S. A. Syed Asif, O. L. Warren, D. C. Chrzan, A. M. Minor, A. P. Alivisatos, *Nat. Mater.* **2008**, *7*, 947.

[28] T. Asada, Y. Koyama, *Phys. Rev. B - Condens. Matter Mater. Phys.* **2007**, *75*, DOI 10.1103/PhysRevB.75.214111.

[29] Y. Ivry, D. P. Chu, C. Durkan, *Nanotechnology* **2010**, *21*, DOI 10.1088/0957-4484/21/6/065702.

[30] E. A. Eliseev, A. N. Morozovska, Y. Gu, A. Y. Borisevich, L. Q. Chen, V. Gopalan, S. V. Kalinin, *Phys. Rev. B - Condens. Matter Mater. Phys.* **2012**, *86*, DOI 10.1103/PhysRevB.86.085416.

[31] I. Stolichnov, L. Feigl, L. J. McGilly, T. Sluka, X. K. Wei, E. Colla, A. Crassous, K. Shapovalov, P. Yudin, A. K. Tagantsev, N. Setter, *Nano Lett.* **2015**, *15*, 8049.

[32] W. T. Lee, E. K. H. Salje, *Appl. Phys. Lett.* **2005**, *87*, 1.

[33] X. Ren, Y. Wang, K. Otsuka, P. Lloveras, T. Castán, M. Porta, A. Planes, A. Saxena, *MRS Bull.* **2009**, *34*, 838.

[34] L. Wang, J. Teng, X. Sha, J. Zou, Z. Zhang, X. Han, *Nano Lett.* **2017**, *17*, 4733.

[35] U. Dahmen, R. Erni, V. Radmilovic, C. Ksielowski, M.-D. Rossell, P. Denes, *Philos. Trans. A. Math. Phys. Eng. Sci.* **2009**, *367*, 3795.

[36] A. M. Minor, S. A. Syed Asif, Z. Shan, E. A. Stach, E. Cyrankowski, T. J. Wyrobek, O. L. Warren, *Nat. Mater.* **2006**, *5*, 697.

[37] O. L. Warren, Z. Shan, S. A. S. Asif, E. A. Stach, J. W. Morris, A. M. Minor, *Mater.*

Today **2007**, *10*, 59.

[38] O. L. Warren, S. A. Downs, T. J. Wyrobek, *Zeitschrift für Met.* **2004**, *95*, 287.

[39] C. H. Chiu, C. W. Huang, Y. H. Hsieh, J. Y. Chen, C. F. Chang, Y. H. Chu, W. W. Wu, *Nano Energy* **2017**, *34*, 103.

[40] D. A. Muller, N. Nakagawa, A. Ohtomo, J. L. Grazul, H. Y. Hwang, *Nature* **2004**, *430*, 657.

[41] C. T. Nelson, P. Gao, J. R. Jokisaari, C. Heikes, C. Adamo, A. Melville, S. H. Baek, C. M. Folkman, B. Winchester, Y. Gu, Y. Liu, K. Zhang, E. Wang, J. Li, L. Q. Chen, C. B. Eom, D. G. Schlom, X. Pan, *Science (80-.).* **2011**, *334*, 968.

[42] C. Gammer, V. Burak Ozdol, C. H. Liebscher, A. M. Minor, *Ultramicroscopy* **2015**, *155*, 1.

[43] V. B. Ozdol, C. Gammer, X. G. Jin, P. Ercius, C. Ophus, J. Ciston, A. M. Minor, *Appl. Phys. Lett.* **2015**, *106*, DOI 10.1063/1.4922994.

[44] O. Panova, C. Ophus, C. J. Takacs, K. C. Bustillo, L. Balhorn, A. Salleo, N. Balsara, A. M. Minor, *Nat. Mater.* **2019**, *18*, 860.

[45] C. Ophus, *Microsc. Microanal.* **2019**, *25*, 563.

[46] E. A. Stach, D. Zakharov, R. D. Rivas, P. Longo, M. Lent, A. Gubbens, C. Czarnik, *Microsc. Microanal.* **2013**, *19*, 392.

[47] A. Myasnikov, S. Zheng, D. Bulkley, Y. Cheng, D. Agard, *Microsc. Microanal.* **2018**, *24*, 890.

[48] T. C. Pekin, C. Gammer, J. Ciston, C. Ophus, A. M. Minor, *Scr. Mater.* **2018**, *146*, 87.

[49] C. Gammer, T. C. Pekin, C. Ophus, A. M. Minor, J. Eckert, in *ICTAEM 2018 Proc. First Int. Conf. Theor. Appl. Exp. Mech.*, Springer, Cham, **2018**, pp. 356–357.

[50] T. C. Pekin, J. Ding, C. Gammer, B. Ozdol, C. Ophus, M. Asta, R. O. Ritchie, A. M. Minor, *Nat. Commun.* **2019**, *10*, DOI 10.1038/s41467-019-10416-5.

[51] I. J. Johnson, K. C. Bustillo, J. Ciston, B. R. Draney, P. Ercius, E. Fong, A. Goldschmidt, J. M. Joseph, J. R. Lee, A. M. Minor, C. Ophus, A. Selvarajan, D. E. Skinner, T. Stezelberger, C. S. Tindall, P. Denes, *Microsc. Microanal.* **2018**, *24*, 166.

[52] T. C. Pekin, C. Gammer, J. Ciston, C. Ophus, A. M. Minor, *Scr. Mater.* **2018**, *146*, 87.

[53] C. Gammer, J. Kacher, C. Czarnik, O. L. Warren, J. Ciston, A. M. Minor, *Appl. Phys. Lett.* **2016**, *109*, DOI 10.1063/1.4961683.

[54] Y. Lu, Y. Ganesan, J. Lou, *Exp. Mech.* **2010**, *50*, 47.

[55] Y. Lu, C. Peng, Y. Ganesan, J. Y. Huang, J. Lou, *Nanotechnology* **2011**, *22*, 355702.

[56] H. Guo, K. Wang, Y. Deng, Y. Oh, S. A. Syed Asif, O. L. Warren, Z. W. Shan, J. Wu, A. M. Minor, *Appl. Phys. Lett.* **2013**, *102*, DOI 10.1063/1.4810872.

[57] S. Bhowmick, H. Espinosa, K. Jungjohann, T. Pardoen, O. Pierron, *MRS Bull.* **2019**, *44*, 487.

[58] R. Ramachandramoorthy, W. Gao, R. Bernal, H. Espinosa, *Nano Lett.* **2016**, *16*, 255.

[59] L. Zeng, C. Gammer, B. Ozdol, T. Nordqvist, J. Nygård, P. Krogstrup, A. M. Minor, W. Jäger, E. Olsson, *Nano Lett.* **2018**, *18*, 4949.

[60] N. T. Tsou, P. R. Potnis, J. E. Huber, *Phys. Rev. B - Condens. Matter Mater. Phys.* **2011**, *83*, DOI 10.1103/PhysRevB.83.184120.

[61] T. Sluka, A. K. Tagantsev, P. Bednyakov, N. Setter, *Nat. Commun.* **2013**, *4*, DOI 10.1038/ncomms2839.

[62] M. Y. Gureev, A. K. Tagantsev, N. Setter, *Phys. Rev. B - Condens. Matter Mater. Phys.* **2011**, *83*, DOI 10.1103/PhysRevB.83.184104.

[63] J. X. Zhang, B. Xiang, Q. He, J. Seidel, R. J. Zeches, P. Yu, S. Y. Yang, C. H. Wang, Y. H. Chu, L. W. Martin, A. M. Minor, R. Ramesh, *Nat. Nanotechnol.* **2011**, *6*, 98.

[64] P. Gao, J. Britson, J. R. Jokisaari, C. T. Nelson, S. H. Baek, Y. Wang, C. B. Eom, L. Q. Chen, X. Pan, *Nat. Commun.* **2013**, *4*, DOI 10.1038/ncomms3791.

[65] O. Panova, X. C. Chen, K. C. Bustillo, C. Ophus, M. P. Bhatt, N. Balsara, A. M. Minor, *Micron* **2016**, *88*, 30.

[66] C. Ophus, P. Ercius, M. Huijben, J. Ciston, *Appl. Phys. Lett.* **2017**, *110*, DOI 10.1063/1.4975932.

[67] J. Ciston, C. Ophus, P. Ercius, H. Yang, R. dos Reis, C. T. Nelson, S.-L. Hsu, C. Gammer, B. V. Özdöl, Y. Deng, A. Minor, *Microsc. Microanal.* **2016**, *22*, 1412.

[68] J. Ciston, I. J. Johnson, B. R. Draney, P. Ercius, E. Fong, A. Goldschmidt, J. M. Joseph, J. R. Lee, A. Mueller, C. Ophus, A. Selvarajan, D. E. Skinner, T. Stezelberger, C. S. Tindall, A. M. Minor, P. Denes, *Microsc. Microanal.* **2019**, *25*, 1930.

[69] C. Gammer, C. Ophus, T. C. Pekin, J. Eckert, A. M. Minor, *Appl. Phys. Lett.* **2018**, *112*, 171905.

[70] A. M. Minor, *Microsc. Microanal.* **2018**, *24*, 964.

[71] P. S. Phani, K. E. Johanns, G. Duscher, A. Gali, E. P. George, G. M. Pharr, *Acta Mater.* **2011**, *59*, 2172.

[72] J. Wang, S. X. Mao, *Extrem. Mech. Lett.* **2016**, *8*, 127.

[73] J. Wang, Z. Zeng, C. R. Weinberger, Z. Zhang, T. Zhu, S. X. Mao, *Nat. Mater.* **2015**,

14, 594.

[74] L. Liu, J. Wang, S. K. Gong, S. X. Mao, *Sci. Rep.* **2014**, *4*, 4397.

[75] Y. Deng, C. Gammer, J. Ciston, P. Ercius, C. Ophus, K. Bustillo, C. Song, R. Zhang, D. Wu, Y. Du, Z. Chen, H. Dong, A. G. Khachaturyan, A. M. Minor, *Acta Mater.* **2019**, DOI 10.1016/j.actamat.2019.10.018.

[76] M. Legros, *Comptes Rendus Phys.* **2014**, *15*, 224.

[77] T. Sato, L. Jalabert, H. Fujita, *Microelectron. Eng.* **2013**, *112*, 269.

[78] H. D. Espinosa, R. A. Bernal, T. Filleter, *Small* **2012**, *8*, 3233.

[79] H. D. Espinosa, Yong Zhu, N. Moldovan, *J. Microelectromechanical Syst.* **2007**, *16*, 1219.

[80] B. Pant, B. L. Allen, T. Zhu, K. Gall, O. N. Pierron, *Appl. Phys. Lett.* **2011**, *98*, 053506.

[81] H. Guo, M. I. Khan, C. Cheng, W. Fan, C. Dames, J. Wu, A. M. Minor, *Nat. Commun.* **2014**, *5*, DOI 10.1038/ncomms5986.

[82] K. Bhattacharya, R. D. James, *Science (80-.).* **2005**, *307*, 53.

[83] M. J. Polking, M. G. Han, A. Yourdkhani, V. Petkov, C. F. Kisielowski, V. V. Volkov, Y. Zhu, G. Caruntu, A. Paul Alivisatos, R. Ramesh, *Nat. Mater.* **2012**, *11*, 700.

[84] A. Barnoush, P. Hosemann, J. Molina-Aldareguia, J. M. Wheeler, *MRS Bull.* **2019**, *44*, 471.

[85] J. Sun, L. He, Y.-C. Lo, T. Xu, H. Bi, L. Sun, Z. Zhang, S. X. Mao, J. Li, *Nat. Mater.* **2014**, *13*, 1007.

[86] Q. Yu, L. Qi, T. Tsuru, R. Traylor, D. Rugg, J. W. Morris, M. Asta, D. C. Chrzan, A. M. Minor, *Science (80-.).* **2015**, *347*, 635.
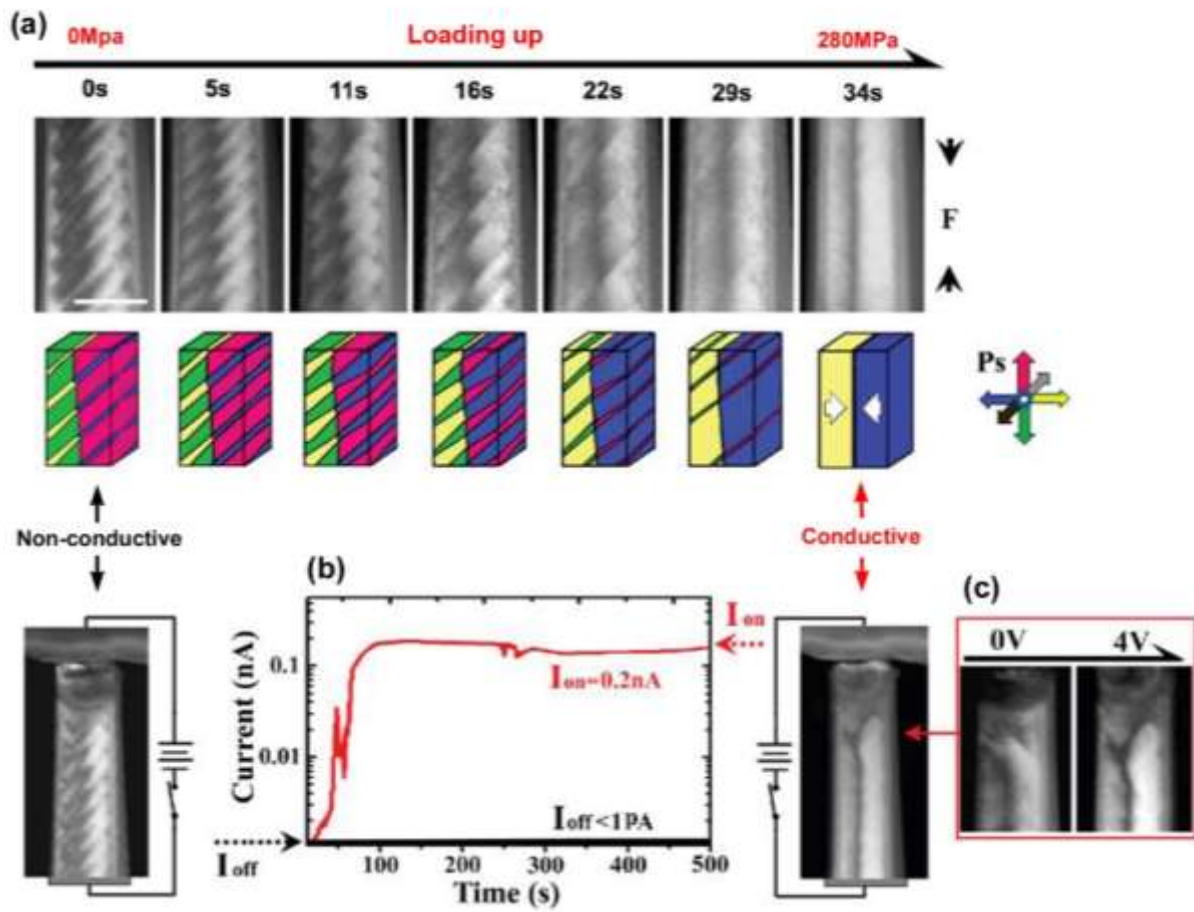
WILEY-VCH

Figure 1. (a) The domain evolutions in a single-crystal BaTiO$_3$ nanopillar under quantitative compression loading: from a herringbone domain structure to a charged head-to-head 180$^{-degree}$ domain structure. (b) The dramatically enhanced conductivity related to the domain structure changing, i.e. the conductivity induced by a free-electron gas structure. (c) The head-to-head 180-degree domain wall does not reach the pillar-top electrodes until a 4V electric field between the top and bottom electrodes has been applied. The scale bar in (a) is 100nm.
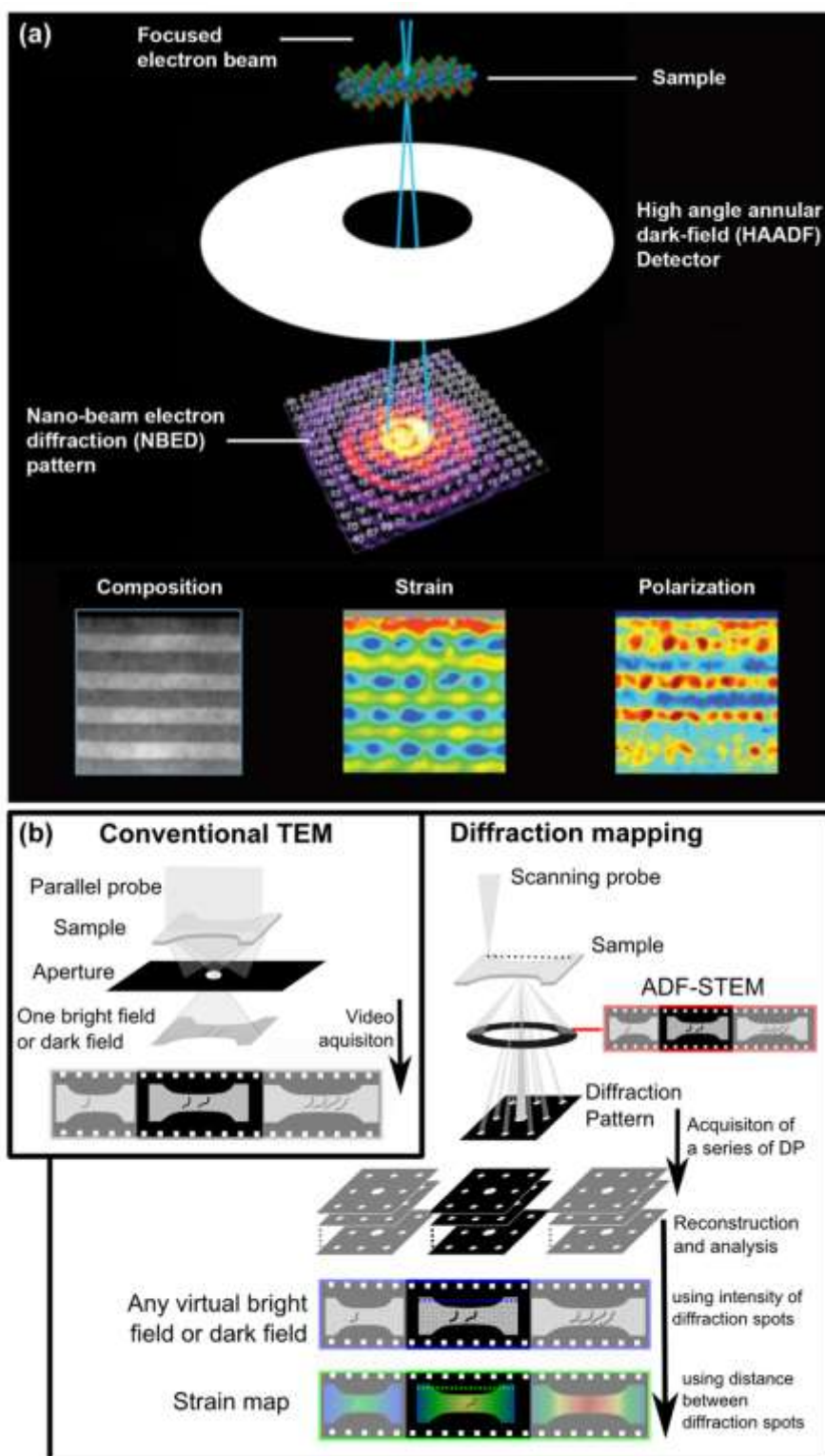
Figure 2. *In-situ* observation by 4D-STEM. (a) The principle of the high-throughput multi-channel 4D-STEM mapping, with a case of a $SrTiO_3$/$PbTiO_3$ multilayer heterojunction structure. Figures are reproduced with permission[67]. (b) A schematic demonstrating the difference of TEM *in-situ* nanomechanical testing conducted in conventional TEM mode and in dynamic 4D-STEM mode, emphasizing the multi-contrast capability of 4D-STEM. Figures are reproduced with permission[70].
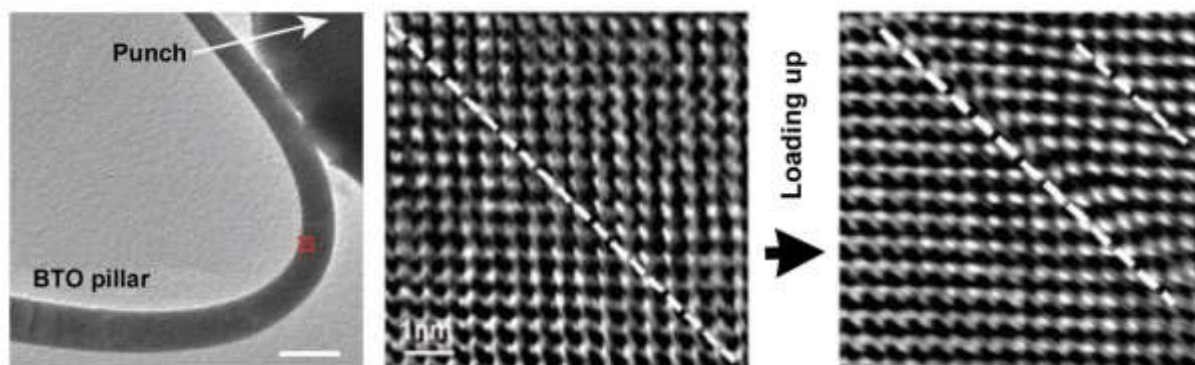
Figure 3. Defect nucleation at a 90-degree domain wall in single-crystal BaTiO₃ nanopillar under heavy shear (~2GPa) which leads to cracking. Here, we highlight the sharp 90-degree domain wall with a single white dashed line, and the broadened domain wall under heavy shear with two white dashed lines, respectively.
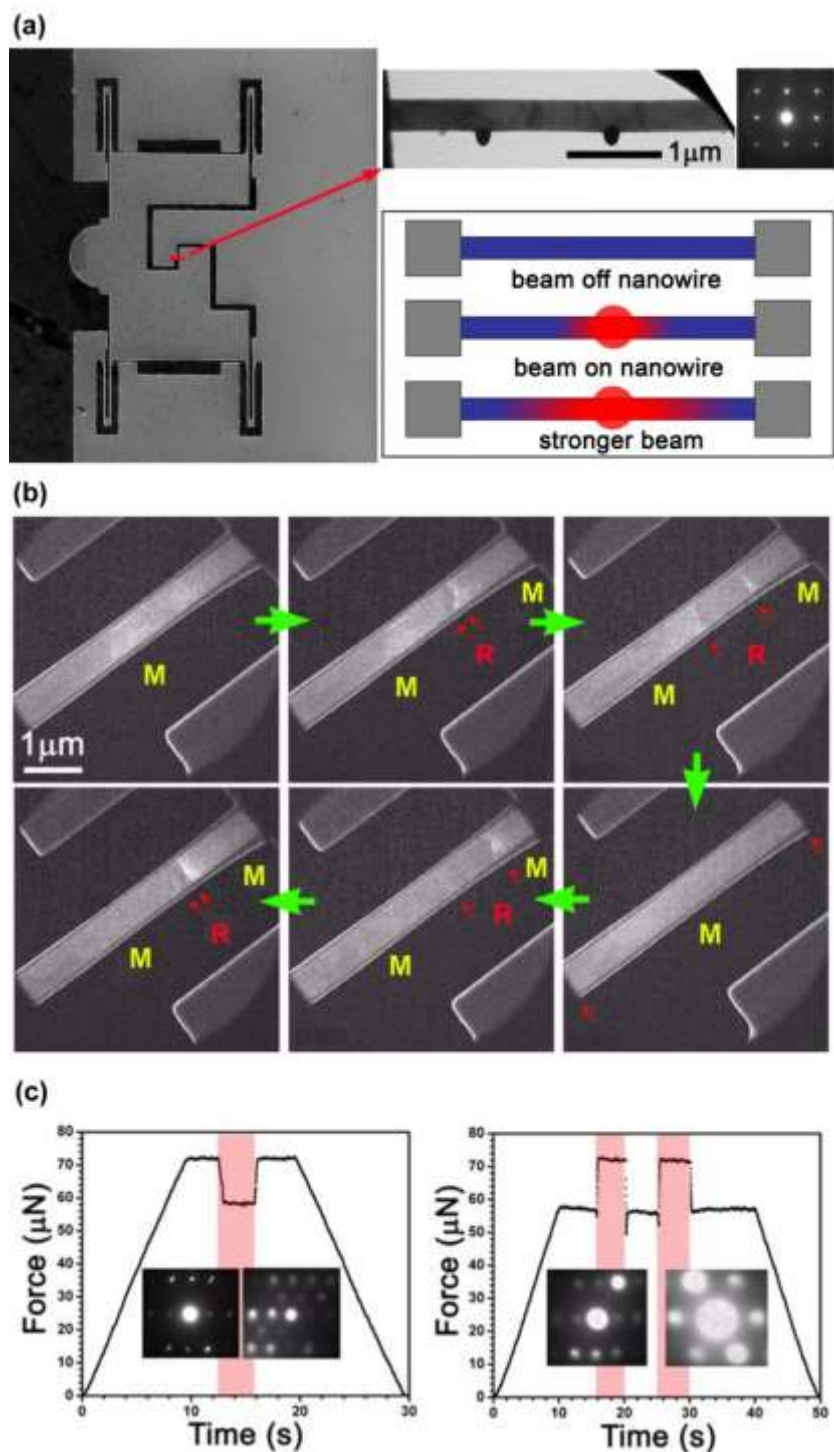
Figure 4. The strain and force output of a VO$_2$ nanowire under electron beam heating, being measured *in-situ* by a MEMS PtP chip. (a) The PtP device and the VO$_2$ nanowire on it. The local phase transformation under heating causes a strain and force output, which can be well detected by the *in-situ* mechanical TEM system with the PtP device. (b) The *in-situ* dark-field observations of the nanowire, displaying local phase transition during a heating-and-cooling process. (c) The force output depending on the local phase transformation. Figures are reproduced with permission[56].
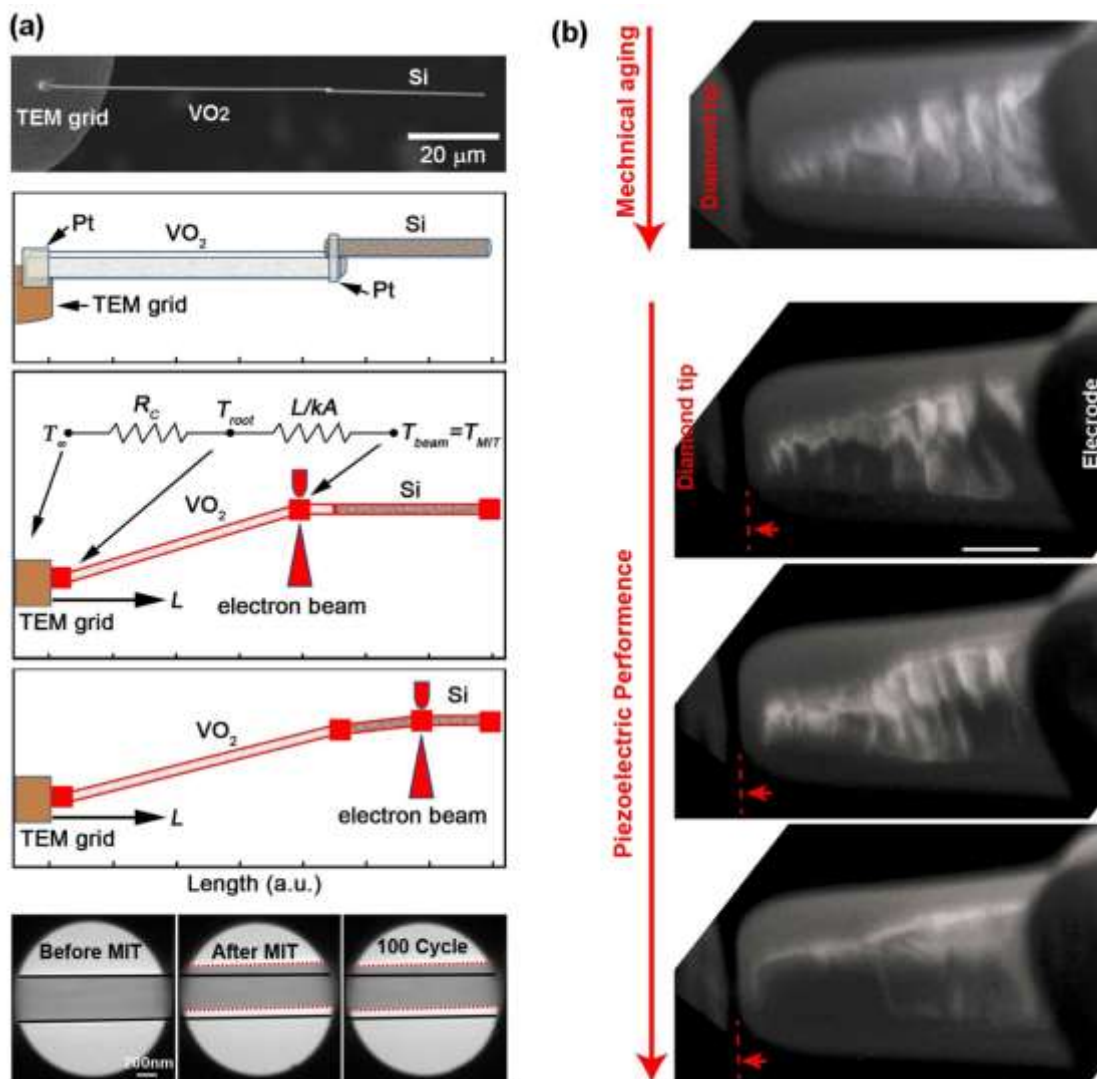
Figure 5. (a) A VO$_2$ nanowire-based nano-thermometer which can quantitatively evaluate the temperature increase caused by electron beam heating. Its setup (SEM image, see upper inset), working principle (see middle three insets), and *in-situ* TEM observation of the strain outputs under electron beam heating/cooling cycling (before and after MIT for the first cycle, and after MIT for the 100th cycle. See three lower insets) are shown in the insets. Figures are reproduced with permission[81]. (b) The *in-situ* observation of a BaTiO$_3$ nanopillar under a mechanical aging (i.e. under a compression for a 100mins. See upper inset) and the piezoelectric performance of the BaTiO$_3$ pillar (the electric field is applied between the diamond tip and bottom electrode. See three lower insets) after the aging. The scale bar is 100 nm.